 FDMP, vol.13, no.4, pp.235-249, 2017

Numerical Simulation of Thermosolutal Convective Transitions in a Very Narrow Porous Annulus under the Influence of Lewis Number

A. Ja[1] and A. Cheddadi[1]

Abstract: This paper reports on the natural convection within a very narrow horizontal annular cavity filled with a porous medium saturated by a binary fluid. The main objective of this study is the identification of the effect of Lewis number on the flow structure and on the heat and mass transfer rates, in a cavity of very small radius ratio R=1.05, in the case of equal buoyancy forces (N=1), for a Rayleigh number Ra=50. The dimensionless governing equations were solved by the centered Finite Difference method using the ADI scheme. Several multicellular flows appear during the variation of the Lewis number, resulting in a direct impact on the heat and solutal transfer rates.

Keywords: Thermosolutal convection, Porous medium, Annular geometry, Finite Difference, Critical Lewis number.

Nomenclature

D	Mass diffusivity, $m^2 s^{-1}$
g	Gravitational acceleration, $m s^{-2}$
K	Permeability of the porous medium, m^2
r	Dimensionless radial coordinate
T, S	Dimensionless temperature and concentration
u, v	Dimensionless velocity in r and φ directions

Greek Symbols

α	Thermal diffusivity, $m^2 s^{-1}$
β	Expansion coefficient, K^{-1}
Ψ	Dimensionless stream function
ν	Kinematic viscosity, $m^2 s^{-1}$
φ	Polar angle, rad
ρ	Density, $kg m^{-3}$

Subscripts

0	Reference value
i	Inner cylinder

[1] Research Team "Thermal Systems and Real Flows", Mohammadia School of Engineers, Mohammed V University in Rabat, Morocco.

o	Outer cylinder
T	Thermal
S	Solutal

Exponents

n	Iteration number
C^+	Counterclockwise cell
C^-	Clockwise cell

Operators

∇^2 $\quad \nabla^2 = \frac{1}{r}\frac{\partial}{\partial r}\left(r\frac{\partial}{\partial r}\right)+\frac{1}{r^2}\frac{\partial^2}{\partial \varphi^2}$

∇ $\quad \nabla=\frac{\partial}{\partial r}\vec{e}_r+\frac{1}{r}\frac{\partial}{\partial \varphi}\vec{e}_\varphi$

Non-dimensional Numbers

Le	Lewis number, [α /D]
N	Buoyancy ratio, [$\beta_S \Delta S / \beta_T \Delta T$]
R	Radii ratio, [r_o / r_i]
Ra	Darcy-Rayleigh number, [$g \beta_T \Delta T K r_i / \upsilon \alpha$]

1 Introduction

Natural convection in porous media induced by a simultaneous application of temperature and concentration gradients, named double-diffusive or thermosolutal, has undergone less attention compared to the natural thermal convection, despite its importance in different technological and industrial fields, e.g. in dissemination of chemical particles in chemical reactors packed bed, the spread of radioactive substances in nuclear deposits under land, desalination of sea water, separation of species etc.

The published literature on thermosolutal convection in porous media was dedicated mainly to the square and rectangular cavities. Among many numerical, experimental and analytical studies, we can cite the investigation on a square porous cavity where the horizontal walls are subjected to constant temperatures and concentrations by Trevisan et al. [Trevisan and Bejan (1985)]. The numerical solution shows that, for the purely thermal case (N=0), the variation of the Lewis number has no influence on the rate of thermal transfer. Contrariwise, the solutal transfer rate increases with increasing *Le*. A method of scale analysis was used and provided a description of the phenomenon of natural convection for the two important cases, namely, heat transfer driven flows and mass transfer driven flows, in order to predict the average heat and mass transfer rates and their respective domains of validity. Furthermore, the comparison between the results obtained for both methods has shown a good agreement. These techniques were used by the same authors [Trevisan and Bejan (1986)] to study the thermosolutal convection in a rectangular porous cavity subjected to uniform heat and mass fluxes imposed horizontally. In Bourich

et al. [Bourich, Amahmid and Hasnaoui (2004)] the natural convection in a square porous cavity subjected to cross temperature and concentration gradients was studied. The numerical study aimed to extract the influence of governing parameters and led to simple correlations between the critical Rayleigh number and the Lewis number.

The case of vertical cylindrical cavity subjected to uniform heat and solutal fluxes on the side wall, was studied numerically by Marcoux et al. [Marcoux, Charrier-Mojtabi and Azaiez (2011)]. The influence of the governing parameters on the heat and mass transfer rates has been investigated. Increasing the Lewis number leads to a progressive decrease in the average Nusselt number, unlike, the average Sherwood number which increases with increasing Lewis number. The same problem was considered in Kalita et al. [Kalita and Dass (2011)], in the case where the side walls are subjected to constant and uniform temperatures and solutal concentrations. The numerical analysis was carried out in this study by a Higher Order Compact (HOC) method and has shown that increasing the Lewis number had a negligible effect on the temperature distribution in the case of cooperating forces. While the concentration in the center of the cavity is uniform, the solutal boundary layers become thinner as the Lewis number is increased.

In the case of horizontal cylindrical annular cavity submitted to simultaneous application of temperature and concentration gradients, the phenomenon of convection in the presence of the Soret effect was investigated in Alloui et al. [Alloui and Vasseur (2011)] for constant values of Lewis number Le=2 and radii ratio R=2. The study proved numerically the existence of critical values of buoyancy ratio leading to two types of solutions. Recently, the study of the influence of various parameters of the thermosolutal natural convection on the flow structure and on the thermal and solutal transfer rates has been investigated in Ja et al. [Ja, Belabid and Cheddadi (2015)], for a fixed radius ratio R=2, in the case of cooperating volume forces.

In such problems, the appearance of multicellular flows depends essentially on the geometry of the cavity and is characterized by critical values of the Rayleigh number initiating thermal instabilities (Rayleigh-Benard type natural convection). Much studies concerning purely thermal convection in porous horizontal annular cavities have shown the critical values of Rayleigh number associated with the appearance of multicellular flows and sometimes gave correlations describing the heat transfer rate as a function of Rayleigh number Caltagirone et al. [Caltagirone (1976); Caltagirone (1978); Charrier-Mojtabi (1997); Rao, Fukuda and Hasegawa (1987); Barbosa Mota and Saatdjian (1994); Barbosa Mota and Saatdjian (1997); Hamad and Khan (1998); Alfahaid, Sakr and Ahmed (2005); Belabid and Cheddadi (2014)]. On the other hand, the onset and development of thermosolutal multicellular flows was investigated in a rectangular cavity filled with a porous medium saturated by a binary fluid, by Charrier-Mojtabi et al. [Charrier-Mojtabi, Karimi-Fard, Azaiez et al. (1998)] for constant temperatures and concentrations on the vertical sides, and Amahmid et al. [Amahmid, Hasnaoui, Mamou et al. (1999)] for a cavity subjected to uniform heat and mass fluxes on the horizontal walls. The critical Rayleigh number was evaluated, in both studies, over large ranges of the thermosolutal parameters (Le, N).

Recently, great interest has been shown in the experimental determination of the Soret, thermodiffusion and molecular diffusion coefficients of mixtures, resulting in useful

worldwide benchmarks (see e.g. [Bou-Ali, Ahadi, Alonso de Mezquia et al. (2015)] for ternary mixtures).

In this paper, we present a numerical simulation of the effect of variation of the Lewis number on the thermosolutal convection, in an annular space delimited by two coaxial, horizontal, isotherm and impermeable cylinders. We are primarily interested in the appearance of multicellular flows. The annulus is filled with a porous medium saturated by a binary fluid. The inner and outer cylinders of radius ratio respectively r_i and r_o are maintained at constant and uniform temperatures and concentrations, T_i, S_i and T_o, S_o respectively for the inner and outer cylinders, with $T_i>T_o$ and $S_i>S_o$, as shown in Figure 1. The binary fluid is assumed to be Newtonian, incompressible and satisfying Boussinesq approximation: $\rho=\rho_0\,[1-\beta_T\,(T-T_0)-\beta_S\,(S-S_0)]$, where β_T and β_S are the thermal and solutal expansion coefficients, respectively. T_0 and S_0 are the reference temperature and concentration. All the results are presented for a narrow cavity of radius ratio R=1.05, in the case of a buoyancy ratio N=1, a Darcy-Rayleigh number Ra=50, and Lewis numbers in the wide range $0.1\leq Le\leq 1000$, where: $Ra=\dfrac{g\beta_T\Delta T K r_i}{\nu\alpha}$, $N=\dfrac{\beta_S\Delta S}{\beta_T\Delta T}$, $Le=\dfrac{\alpha}{D}$ and $R=\dfrac{r_o}{r_i}$, ΔT being the temperature difference T_i-T_o, and ΔS the concentration difference. In practice, the Lewis number value is much smaller than the considered range in this study. However, in order to understand the influence of this parameter and study the behavior of the binary fluid in asymptotic situations ($Le\to\infty$ and $Le\to 0$) very high theoretical Lewis number values are investigated.

2 Mathematical formulation

The dimensionless steady state equations governing the two-dimensional flow described in stream function formulation are given by:

$$\nabla^2\,\psi=-Ra\left[\left(\sin\varphi\frac{\partial T}{\partial r}+\frac{\cos\varphi}{r}\frac{\partial T}{\partial\varphi}\right)+N\left(\sin\varphi\frac{\partial S}{\partial r}+\frac{\cos\varphi}{r}\frac{\partial S}{\partial\varphi}\right)\right] \tag{1}$$

$$\left(\vec{V}.\nabla\right)T=\nabla^2 T \tag{2}$$

$$\left(\vec{V}.\nabla\right)S=Le^{-1}\,\nabla^2 S \tag{3}$$

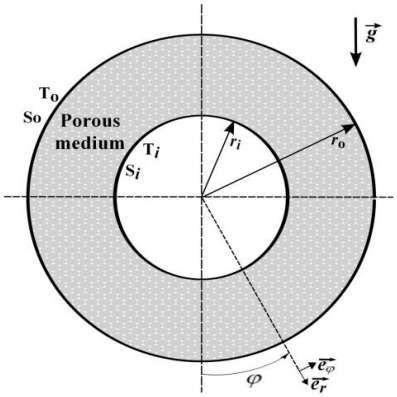

Figure 1: Schematic diagram of the annular domain

where r is the dimensionless radial coordinate and φ is the polar angle measured from the downward vertical, T and S are the dimensionless temperature and concentration, Ψ is the stream function defined by $u = \frac{1}{r}\frac{\partial \psi}{\partial \varphi}$ and $v = -\frac{\partial \psi}{\partial r}$, where u and v are respectively the radial and tangential velocities.

The governing equations reduce to the dimensionless form by using the following reference system: r_i for the radial coordinate, $\frac{\alpha}{r_i}$ for the velocity, ΔT for the temperature and ΔS for the concentration.

The dimensionless boundary conditions for the above system of equation are:

For r=1 : T=1, S=1 and $\frac{\partial \psi}{\partial \varphi} = 0$, $\forall \varphi$ (4)

For r=R : T=0, S=0 and $\frac{\partial \psi}{\partial \varphi} = 0$, $\forall \varphi$ (5)

Taking into account the symmetry of the problem, two additional boundary conditions are introduced:

For φ =0, π : $\frac{\partial T}{\partial \varphi} = 0$ and $\frac{\partial \psi}{\partial r} = 0$, $\forall r$ (6)

The heat and mass transfer rates are evaluated on the inner cylinder. The local Nusselt and Sherwood numbers are defined respectively by:

$$Nu_l = -\ln R \left.\frac{\partial T}{\partial r}\right|_{r=1} \quad \text{and} \quad Sh_l = -\ln R \left.\frac{\partial S}{\partial r}\right|_{r=1} \tag{7}$$

The average Nusselt and Sherwood numbers considering the half annular space are defined as follows:

$$\overline{Nu} = \frac{1}{\pi}\int_0^\pi Nu_l \, d\varphi \quad \text{and} \quad \overline{Sh} = \frac{1}{\pi}\int_0^\pi Sh_l \, d\varphi \tag{8}$$

3 Numerical method

The governing equations are discretized using a centered Finite Difference method. An iterative procedure is performed with the Alternating Direction Implicit scheme (ADI). The process is completed when the following criterion is satisfied in each node of the grid: $\frac{\chi_{i,j}^{n+1} - \chi_{i,j}^{n}}{\chi_{i,j}^{n}} \leq 10^{-8}$, where χ refers to T, S and Ψ and n denotes the reached iteration number, the subscript (i,j) represents a grid node. Preliminary tests conducted to examine the effect of the grid size on the results showed that a 91 ×111 grid is sufficient. The accuracy of the numerical code was compared with available data in the case of pure thermal convection for R=2. As listed in Table 1, an extremely good agreement between our numerical and literature results using different numerical methods. In addition, a comparison between our study with the available results of Himasekhar et al. [Himasekhar and Bau (1988); Charrier-Mojtabi (1991)] is carried out for narrow cavities (see Table 2), and they are also found to be in excellent agreement.

The numerical investigation is performed with introduction of pure conduction stream function, temperature and concentration fields as initial conditions:

$$T_{i,j}^{0} = S_{i,j}^{0} = 1 - \frac{Log\, r_i}{Log\, R} \quad \text{and} \quad \psi_{i,j}^{0} = 0 \tag{9}$$

Table 1: Comparison of the average Nusselt number with literature for R=2, N=0

Study	Numerical methods	*Ra*		
		50	100	150
Caltagirone (1976)	Galerkin	1.3278	1.8286	---
Bau (1984)	Perturbation	1.335	1.844	2.295
Charrier-Mojtabi (1997)	Fourier-Galerkin	1.334	1.867	2.309
Belabid and Cheddadi (2014)	Samarskii-Andreev	1.3440	1.8687	---
This study	ADI	1.3429	1.8677	2.3114

Table 2: Comparison with Fourier-Galerkin method for narrow cavities for N=0

Ra	*R*	Himasekhar and Bau (1988)	Charrier-Mojtabi (1991)	This study
100	$2^{1/4}$	1.0045	1.0045	1.0045
200		1.0177	1.0177	1.0177
100	$2^{1/8}$	1.000288	1.000258	1.000259
200		1.001063	1.001030	1.001034
500		1.006456	1.006425	1.006428

4 Results and discussion

4.1 Flow structure

Figure 2 displays the flow pattern, isotherms and iso-concentration lines in the annular cavity. To give a better visualization of the multicellular flows that appear in the top of the cavity a section zoom $\frac{3\pi}{4} \le \varphi \le \pi$ is used. A progressive change in the Lewis number shows that different types of flow develop successively. First, a unicellular flow dominates all values of $Le \le 31$, with a counterclockwise cell C^+ occupying the entire left half annular space (the flow is symmetrical with respect to the vertical plane passing through the axis of cylinders). A small increase of Lewis number to $Le=31.1$ involves a transition from unicellular to bicellular flow C^+C^-, characterized by a small clockwise cell in the upper part of the annulus, as shown in the subfigure 2a. This bicellular flow transits with the increase of Lewis number to a bicellular swirling flow $C^+c^+C^-$ (subfigure 2b), characterized by the pinching of the main C^+ cell at the value $Le=31.7$, giving rise to a counterclockwise vortex C^+c^+ at the top of this cell. This pattern occurs in the range $31.7 \le Le \le 50.1$. Increasing the Lewis number to the value $Le=50.2$ generates the separation of the vortex C^+c^+ becoming an independent cell, and the creation of a clockwise cell between the corotative cells, giving rise to a tetracellular flow $C^+C^-C^+C^-$ over the whole range $50.2 \le Le \le 136$ (subfigure 2c). Beyond the last value, the system under investigation bifurcates from steady to unsteady state at the critical value $Le=136.1$. On the other hand, another bifurcation occurs at $Le=142$, where the system returns to the steady state with a bicellular structure C^+C^-, characterized by a very small clockwise cell in the upper part of the annulus, as illustrated in the subfigure 2d. This flow pattern persists over the whole range $142 \le Le \le 241$. A second bifurcation to the unsteady flow takes place at $Le=241.1$ and the same behavior is kept in the range $241.1 \le Le \le 457.9$. At the critical value $Le=458$ the unsteady flow tends to return to the unicellular flow C^+ (subfigure 2e), occurring over the large range $458 \le Le \le 1000$.

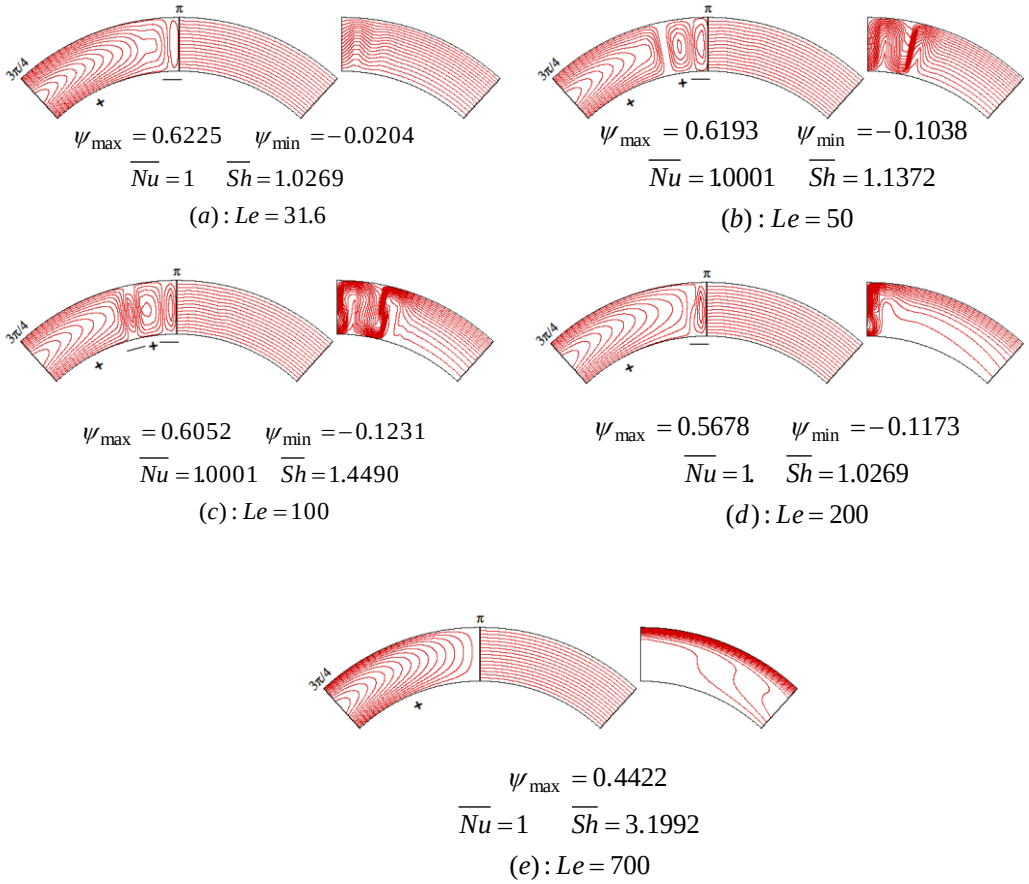

Figure 2: Flow patterns for different values of Lewis number
Streamlines (left), isotherms (center) and isoconcentration lines (right)

4.2 Flow intensity

Figure 3 illustrates the variation of flow intensity represented by the maximum stream function, ψ_{max}, corresponding to the counterclockwise cells and the minimum stream function, ψ_{min}, corresponding to the clockwise cells, as function of Lewis number. The depicted values in the figure show the critical Lewis number characterizing each transition. The above descriptions of the flow structure of different regimes explain clearly the variation of the stream function with the increase in the Lewis number. It is noted that whatever the nature of the flow structure obtained, the gradual increase in the Lewis number causes a progressive decrease in ψ_{max}. The physical meaning for this behavior lies in the thicker dynamic boundary layer for high value of Lewis number (keeping *N* constant), thereby decreasing velocity gradient near the active walls.

Beyond the critical value *Le*=31.1, where the flow is unicellular C^+ (ψ_{min} =0), gradual increase of *Le* leads to the development of the clockwise cells (bicellular C^+C^-, bicellular

swirling $C^+c^+C^-$ and tetracellular flow $C^+C^-C^+C^-$), which causes the progressive increase of $\psi_{\min}$. Though the transition from the unsteady flow to the bicellular flow C^+C^- generates a decrease in $\psi_{\min}$, comparatively to the value obtained for the tetracellular flow at Le=136 (−22.68%), due to the reduction of the number of clockwise cells. The development of the clockwise cells for $142 \leq Le \leq 148$, leads to an enhancement of $\psi_{\min}$. However, the increasing of Lewis number beyond this value ($148 \leq Le \leq 241$) gives a relatively small decrease in $\psi_{\min}$ (−3.64%). When the system shifts to the steady state solution, after the second unsteady flow, Le=458, the flow pattern is unicellular C^+ characterized by $\psi_{\min}$ =0.

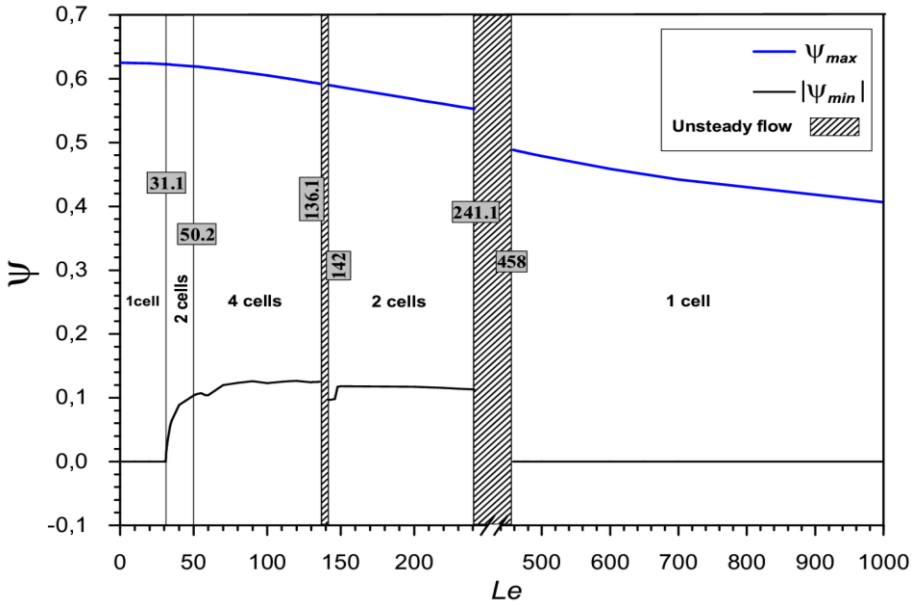

Figure 3: Variation of maximum and minimum stream function as function of Lewis number for Ra=50 and N=1

4.3 Heat and mass transfer rates

In the following section, the flow patterns discussed above are interpreted by means of the local heat and mass transfer rates. Figure 4 illustrates the variation of the local Nusselt number Nu_l, along the inner cylinder for the flow structures described in the previous section. For the unicellular flow $Le \leq 31$, the local heat transfer is identical whatever the Lewis number value, as illustrated in the subfigure 4a, showing that the effect of the Lewis number is negligible on the local heat transfer when the flow pattern is unicellular. For the bicellular flow C^+C^- and bicellular swirling flow $C^+c^+C^-$ (subfigure 2a-b), the variation of the local heat transfer is characterized by four peaks (two maximal and two minimal peaks) in the upper part of the cavity (see subfigure 4b), where the small clockwise cell C^- occurs. The first minimal peak located at the top limit of the largest counterclockwise cell C^+, is due to the transport of the binary fluid from the hot wall to the cold one, giving rise to a minimal local heat transfer. Conversely, at the bottom limit of the small counterclockwise cell c^+ (first maximal peak), the flow is directed from the outer to the inner wall and

promotes the local heat transfer. In the contact zone of the counter-rotating cells c^+C^-, corresponding to the second minimal peak, the flow is directly transported to the cold wall, involving a lower local heat transfer. The last maximal peak located at $\varphi = \pi$, matches the upper limit of the clockwise cell C^-, and the flowing from the cold to the hot cylinder. For the tetracellular flow $C^+C^-C^+C^-$, depicted in subfigure 2c, the same behavior of the local heat transfer discussed for the bicellular flow remains valid, as shown in the subfigure 4c. The two minimal peaks (resp. first maximal peak) are due to the contact zone between the counter-rotating cells C^+C^- (resp. C^-C^+), and the second maximal peak located at the $\varphi = \pi$, is caused by the return of the cooler fluid to the hot wall, as for the bicellular flow. The same principle can apply to the second bicellular flow C^+C^- (subfigure 4d), characterized by a minimal peak corresponding to the contact zone of the counter-rotating cells C^+C^-, and a maximal peak at the top limit of the clockwise cell C^-. Whereas, along the region dominated by the first thermal cell C^+, the local heat transfer remains identical for all values of Lewis number. The theoretical very high Lewis number values considered in the subfigure 4e show no significant influence of the increasing *Le* value on the local heat transfer rate for the unicellular flow.

Figure 5 illustrates the variation of local solutal transfer rate, Sh_l, along the inner cylinder. The previous explanations of the peaks observed at the contact zone of the co-rotating and counter-rotating eddies remain fair for the variation of the local Sherwood number in the multicellular flow case (subfigure 5b-d).

For the unicellular flow characterized by moderate Lewis number values ($Le \leq 31$), a fundamental difference is noted between the local heat and solutal transfer rates (subfigures 4a–5a). It appears that the increasing of the Lewis number enhances the solutal transfer on the inner cylinder within the range $0 \leq \varphi \leq \frac{\pi}{2}$, and a reverse effect is observed for the range $\frac{\pi}{2} \leq \varphi \leq \pi$. Furthermore, in this situation, the solutal transfer is dominated by diffusion, as illustrated by the stratified isoconcentration lines (see subfigure 6a) and the linear dimensionless concentration distribution, shown in the subfigure 7a. An examination of the concentration fields for the unicellular flow obtained for very high Lewis number value (see subfigure 6b where Le=700) indicates that the convection regime dominates the solutal transfer, as can be also confirmed by the concentration distribution in the subfigure 7b.

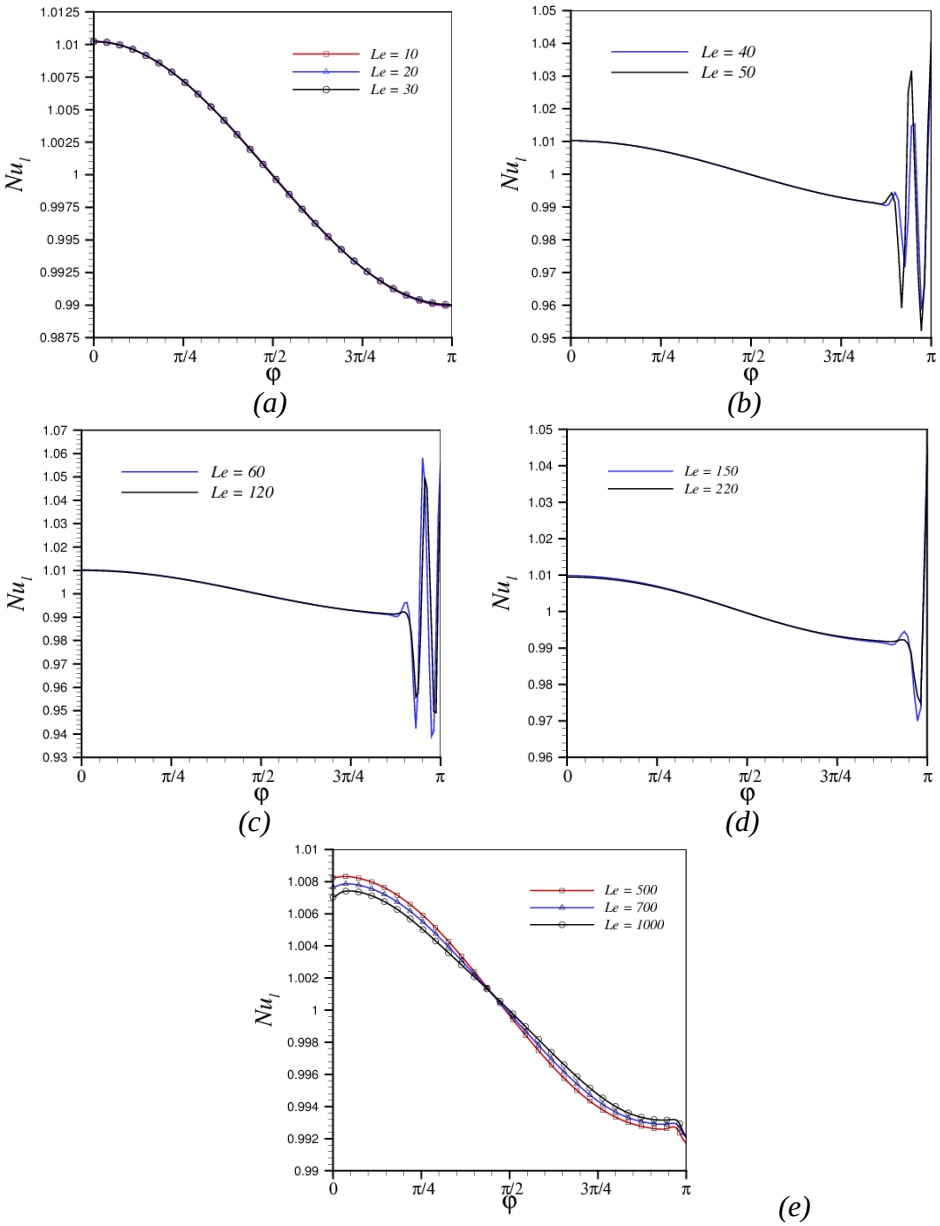

Figure 4: Variation of local Nusselt number along the inner cylinder *(a, e)*: Unicellular flow, *(b, d):* Bicellular flow and *(c):* Tetracellular flow

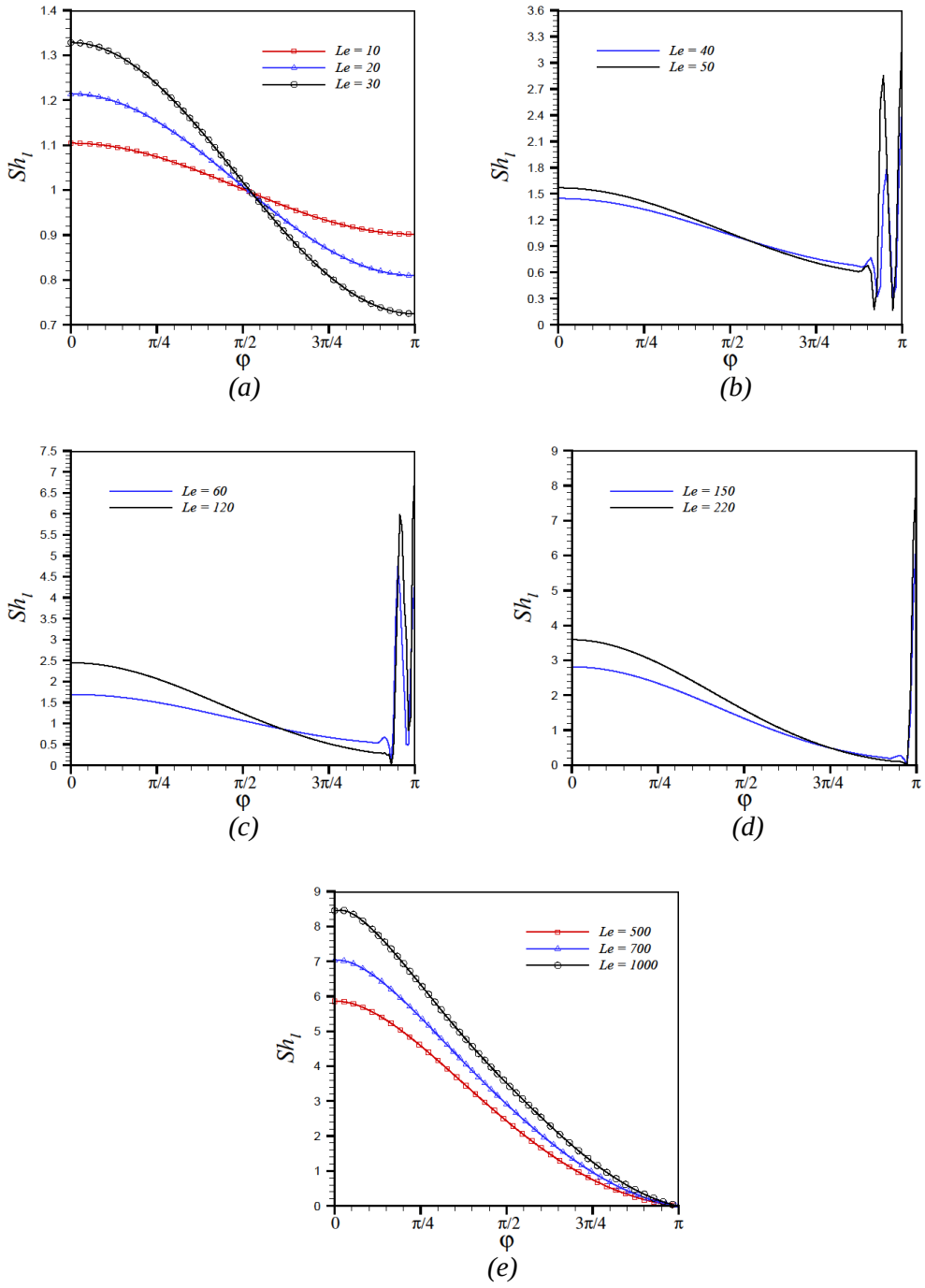

Figure 5: Variation of local Sherwood number along the inner cylinder *(a, e)*: Unicellular flow, *(b, d):* Bicellular flow and *(c):* Tetracellular flow

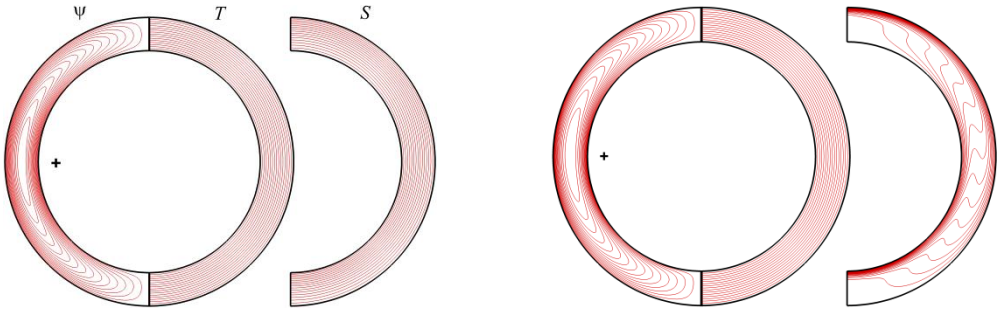

$\psi_{\max} = 0.6228$ $\quad$ $\psi_{\max} = 0.4422$

$\overline{Nu} = 1 \quad \overline{Sh} = 1.0222$ $\quad$ $\overline{Nu} = 1 \quad \overline{Sh} = 3.1992$

$(a): Le = 30$ $\quad$ $(b): Le = 700$

Figure 6: Isocontours of the unicellular flow for *Ra*=50, *N*=1

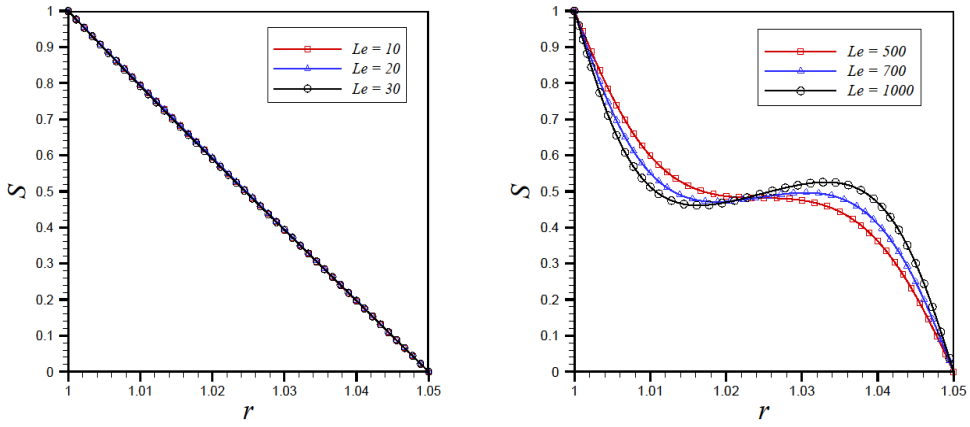

(a) (b)

Figure 7: Dimensionless concentration profile along the radial direction

for *Ra*=50, *N*=1, $\varphi = \frac{\pi}{2}$

Figure 8 shows the variation of the overall Nusselt and Sherwood numbers as a function of Lewis number. The values of Nusselt and Sherwood numbers presented for the unicellular flow are almost of the order of unity. It is therefore concluded, based on the previous results obtained for the local heat and solutal transfer rates, that for very narrow annular cavities and for values of Lewis number $Le \leq 31$, both transfer rates are dominated by conduction / diffusion.

The transition to the multicellular flow characterized by the development of convective cells improves the solutal transfer rate, given the direct transport of particles through the contact zone of the counter-rotating cells. Also, a possible explanation for the average Sherwood number behavior is that the thin solutal boundary layers in the bottom and upper

part respectively near the inner and outer cylinders, promote the solutal transfer. However, the heat transfer rate is still dominated by the conductive mode whatever the value of the Lewis number. The shape of the isotherms shown in Figure 2 and Figure 6 illustrate a radial stratification of the isotherms, when increasing the Lewis number. This allows concluding that the influence of the Lewis number on the thermal distribution is negligible in the narrow cavity, and hence, no influence is noticed on the heat transfer rate.

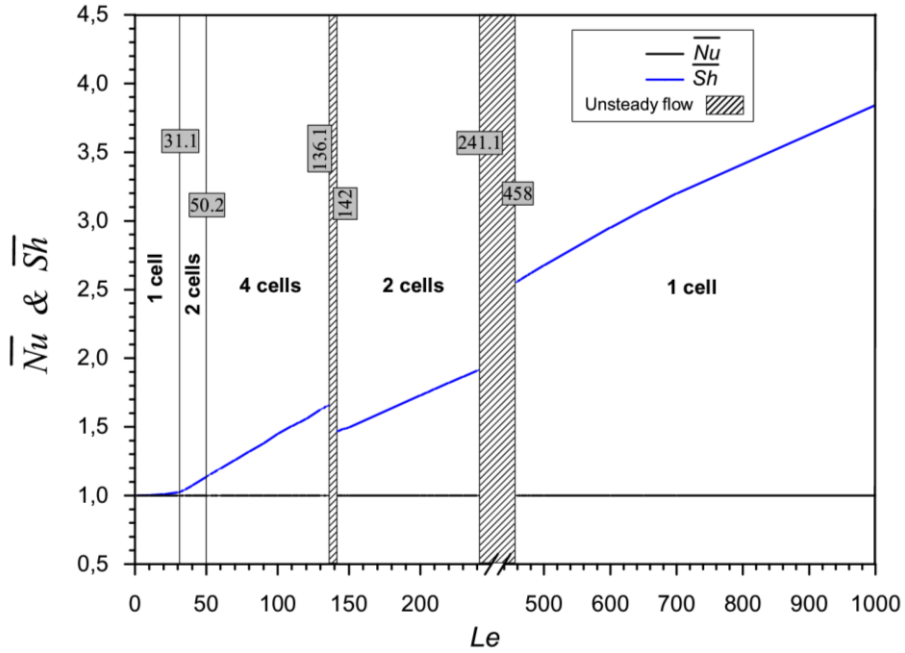

Figure 8: Variation of average Nusselt and Sherwood numbers as function of Lewis number

5 Conclusion

The present investigation is dedicated to the numerical simulation of the steady-state thermosolutal convection in a very narrow horizontal annular enclosure, of radii ratio R=1.05, filled with a porous medium saturated by a binary fluid. A finite difference ADI model is adopted to resolve the governing equations. In particular, the effect of the Lewis number is considered with the constant governing parameters Ra=50 and N=1. The following conclusions have been drawn:

- Different flow patterns (uni- and multi-cellular) occur upon variation of the Lewis number, when initial conditions of pure conduction are used. The ranges of Le characterizing each structure have been determined.
- Unsteady flow occurs in two ranges of Lewis number, i.e, $136.1 \leq Le \leq 141.9$ and $241.1 \leq Le \leq 457.9$.
- The solutal transfer rate increases progressively with increasing Lewis number. Unlike this, the heat transfer is dominated by the conductive regime, with negligible effect of

Lewis number.

References

Alfahaid, A. F.; Sakr, R. Y.; Ahmed, M. I. (2005): Natural convection heat transfer in concentric horizontal annuli containing a saturated porous media. *IIUM Engineering Journal*, vol. 6, no. 1, pp. 41-54.

Alloui, Z.; Vasseur, P. (2011): Natural convection in a horizontal annular porous cavity saturated by a binary mixture. *Computational Thermal Sciences*, vol. 3, no. 5, pp. 407-417.

Amahmid, A.; Hasnaoui, M.; Mamou, M.; Vasseur, P. (1999): Double-diffusive parallel flow induced in a horizontal Brinkman porous layer subjected to constant heat and mass fluxes: analytical and numerical studies. *Heat and Mass Transfer*, vol. 35, no. 4, pp 409-421.

Barbosa Mota, J. P.; Saatdjian, E. (1994): Natural convection in porous horizontal cylindrical annulus. *ASME Journal of Heat Transfer*, vol. 116, pp. 621-626.

Barbosa Mota, J. P.; Saatdjian, E. (1997): On the reduction of natural convection heat transfer in horizontal eccentric annuli containing saturated porous media. *International Journal of Numerical Methods for Heat & Fluid Flow*, vol. 7, no. 4, pp. 401-416.

Bau, H. H. (1984): Low Rayleigh number thermal convection in a saturated porous medium bounded by two horizontal, eccentric cylinders. *Journal of Heat Transfer*, vol. 106, pp. 166-175.

Belabid, J.; Cheddadi, A. (2014): Comparative numerical simulation of natural convection in a porous horizontal cylindrical annulus. *Applied Mechanics and Materials*, vol. 670-671, pp. 613-616.

Bou-Ali, M. M.; Ahadi, A.; Alonso de Mezquia, D; Galand, Q.; Gebhardt, M. et al. (2015): Benchmark values for the Soret, thermodiffusion and molecular diffusion coefficients of the ternary mixture tetralin+isobutylbenzene+n-dodecane with 0.8-0.1-0.1 mass fraction. *The European Physical Journal E*, vol. 38, no. 4.

Bourich, M.; Amahmid, A.; Hasnaoui, M. (2004): Double diffusive convection in a porous enclosure submitted to cross gradients of temperature and concentration. *Energy Conversion & Management*, vol. 45, pp.1655-1670.

Caltagirone, J. P. (1976): Thermoconvective instabilities in a porous medium bounded by two concentric horizontal cylinders. *Journal of fluid Mechanics*, vol. 76, part. 2, pp. 337-362.

Caltagirone, J. P. (1978): Transfert de chaleur par convection naturelle dans une couche poreuse limitée par deux cylindres coaxiaux horizontaux. *International Journal of Refrigeration*, vol. 1, part. 2, Issue 1, pp 13-26.

Charrier-Mojtabi, M. C. (1991): Numerical and experimental study of multicellular free convection flows in an annular porous layer. *International Journal of Heat & Mass Transfer*, vol. 34, no.12, pp. 3061-3074.

Charrier-Mojtabi, M. C. (1997): Numerical simulation of two- and threedimensional free convection flows in a horizontal porous annulus using a pressure and temperature

formulation. *International Journal of Heat and Mass Transfer*, vol. 40, no. 7, pp. 1521-1533.

Charrier-Mojtabi, M. C.; Karimi-Fard, M.; Azaiez, M.; Mojtabi, A. (1998): Onset of a Double-Diffusive Convective Regime in a Rectangular Porous Cavity. *Journal of Porous Media*, vol. 1, pp. 9-17.

Hamad, F. A.; Khan, M. K. (1998): Natural convection heat transfer in horizontal and inclined annulus of different diameter ratios. *Energy Conversion & Management*, vol. 39, no. 8, pp. 797-807.

Himasekhar, K.; Bau, H. H. (1988): Two-dimensional bifurcation phenomena in thermal convection in horizontal, concentric annuli containing saturated porous media. *Journal of Fluid Mechanics*, vol. 187, pp. 267-300.

Ja, A.; Belabid, J.; Cheddadi, A. (2015): Heat and mass transfer in a saturated porous medium confined in cylindrical annular geometry. *International Journal of Mechanical, Aerospace, Industrial and Mechatronics Engineering*, vol. 9, no. 4, pp. 525-529.

Kalita, J. C.; Dass, A. K. (2011): Higher order compact simulation of double-diffusive natural convection in a vertical porous annulus. *Engineering Applications of Computational Fluid Mechanics*, Vol. 5, no. 8, pp. 357-371.

Marcoux, M.; Charrier-Mojtabi, M. C.; Azaiez, M. (1999): Double-diffusive convection in an annular vertical porous layer. *International Journal of Heat and Mass Transfer*, Vol. 42, pp. 2313-2325.

Rao, Y. F.; Fukuda, K.; Hasegawa, S. (1987): Steady and transient analysis of natural convection in a horizontal porous annulus with Galerkin method. *Aiaa/asme Thermophysics Heat Transfer Conference*, vol. 109, pp. 919-927.

Trevisan, O. V.; Bejan, A. (1985): Natural convection with combined heat and mass transfer buoyancy effects in a porous medium. *Journal of Heat and Mass Transfer*, vol. 28, no. 8, pp. 1597-1611.

Trevisan, O. V.; Bejan, A. (1986): Mass and heat transfer by natural convection in a vertical slot filled with porous medium. *International Journal of Heat and Mass*, vol. 29, no. 3, pp. 403-415.